Sensitivity of Arctic clouds to ice microphysical processes in the NorESM2 climate model

Georgia Sotiropoulou[1,2,3], Anna Lewinschal[2], Paraskevi Georgakaki[3], Vaughan Phillips[4], Sachine Patade[4], Annica M. L. Ekman[2], Athanasios Nenes[1,3]

[1]ICE-HT, Foundation for Research and Technology Hellas (FORTH), Patras, Greece
[2]Department of Meteorology, Stockholm University & Bolin Center for Climate Research, Sweden
[3]Laboratory of Atmospheric Processes and their Impacts (LAPI), Ecole Polytechnique Fédérale de Lausanne (EPFL), Lausanne, Switzerland
[4]Department of Physical Geography, University of Lund, Lund, Sweden

Corresponding author: georgia.sotiropoulou@epfl.ch , athanasios.nenes@epfl.ch

Keywords: ice formation, secondary ice production, ice multiplication, Arctic clouds, climate models, Arctic radiation budget

Abstract

Ice formation remains one of the most poorly represented microphysical processes in climate models. While primary ice production (PIP) parameterizations are known to have a large influence on the modeled cloud properties, the representation of secondary ice production (SIP) is incomplete and its corresponding impact is therefore largely unquantified. Furthermore, ice aggregation is another important process for the total cloud ice budget, which also remains largely unconstrained. In this study we examine the impact of PIP, SIP and ice aggregation on Arctic clouds, using the Norwegian Earth System model version 2 (NorESM2). Simulations with both prognostic and diagnostic PIP show that heterogeneous freezing alone cannot reproduce the observed cloud ice and liquid content. The implementation of missing SIP mechanisms (collisional break-up, drop-shattering and sublimation break-up) in NorESM2 improves the modeled ice properties, however results are sensitive to the implementation method. Using an emulated-bin framework, instead of a bulk approach, increases the efficiency of the collisional break-up and drop-shattering processes. Moreover, collisional break-up, which is the dominant SIP mechanism in the examined

conditions, is very sensitive to the treatment of the sublimation correction factor, a poorly-constrained parameter that is included in the utilized parameterization. Finally, ice aggregation is also found to be a critical process; reducing its efficiency (in line with radar observations of shallow Arctic clouds) substantially enhances SIP and further improves the agreement with remote-sensing cloud retrievals. The simulations with enhanced SIP and reduced ice aggregation result in decreased surface downward longwave biases compared to satellite measurements during the cold months.

Significance

Arctic clouds remain a large source of uncertainty in projections of the future climate due to the poor representation of the microphysical processes that govern their life cycle. Ice formation is among the least understood processes. While it is widely recognized that better constraints on primary ice production (PIP) are needed to improve existing parameterizations, we show that secondary ice production (SIP) and ice aggregation can have a more significant impact than PIP on the ice number concentrations. Constraining ice formation through the addition of missing SIP mechanisms and reducing ice aggregation results in improved representation of the cloud macrophysical properties and enhanced total cloud cover in the Arctic region, which in turn contributes to decreased surface downward longwave radiation biases in the cold months.

1. Introduction

Clouds and cloud feedbacks remain the largest source of uncertainty in predictions of the future climate (Boucher et al. 2013). In the most recent Climate Model Intercomparison Project (phase 6 – CMIP6) many general circulation models (GCMs) exhibited larger sensitivity to changes in carbon dioxide concentrations, a metric know as Equilibrium Climate Sensitivity (ECS), compared to CMIP5 models (Zelinka et al. 2020). Murray et al. (2021) showed that ECS values in CMIP6 correlate with mid-to-high latitude low-level cloud feedbacks. Moreover, CMIP6 models suffer from biases in high-latitude cloud cover (Vignesh et al. 2020), cloud radiative impacts (Sledd and L'ecuyer 2020) and snowfall patterns (Thomas et al. 2019).

Mixed-phase clouds, consisting of both supercooled liquid and ice, are the most abundant Arctic cloud type at temperatures between -25^{o}C and 0^{o}C (Shupe et al. 2006; 2011). These clouds are thermodynamically unstable and can easily glaciate through the Wegener-

Bergeron-Findeisen (WBF) mechanism. Moreover, as ice crystals grow through vapor deposition, they can start forming aggregates through collisions with other ice particles or they can gain mass through the collection of liquid droplets (i.e. riming), until they eventually fall out in the form of snow or graupel. Yet, Arctic mixed-phase clouds have been observed to persist for days to weeks (Morrison et al. 2012). Modeling the life-cycle of these clouds is challenging, since errors in the representation of the complex processes that maintain them can lead to rapid glaciation. Predictions of Arctic warming are particularly sensitive to cloud ice formation (Tan et al. 2019). While ice formation processes are likely an important contributor to the CMIP6 spread in predicted mid- and high-latitude cloud feedbacks (Murray et al. 2021), they remain among the most poorly understood microphysical processes in mixed-phase clouds (Seinfeld et al. 2016; Storelvmo 2017).

Primary ice production (PIP) at temperatures above -38^{o}C can only happen heterogeneously in the atmosphere, which means that the assistance of insoluble aerosols that act as Ice Nucleating Particles (INPs) is required (Hoose and Möhler 2012). However, primary ice crystal concentrations can further be enhanced through multiplication processes (Field et al. 2017; Korolev and Leisner 2021), known as secondary ice production (SIP). SIP has received substantially less attention than PIP in the past decades, which is the reason behind its poor (or absent) representation in atmospheric models. Several observational (Gayet et al. 2009; Lloyd et al. 2015; Luke et al. 2021; Pasquier et al. 2022) and modeling (Sotiropoulou et al. 2020; 2021b; Zhao et al. 2021; Zhao and Liu 2021; 2022) studies have indicated that SIP might be particularly important for Arctic clouds, as INP concentrations in the Arctic region are generally low (Wex et al. 2020) to account for the high ice crystal number concentrations (ICNCs) observed.

Several mechanisms that can trigger ice multiplication have been identified in laboratory experiments (Field et al. 2017; Korolev and Leisner 2020), however only one SIP mechanism has until now been considered in GCMs: the Hallett-Mossop (HM) process (Hallett and Mossop, 1974). This is also the case for the Norwegian Earth System model version 2 (NorESM2), which allows HM to occur after cloud drop-snow collisions. However, observational (Rangno and Hobbs 2001; Schwarzenboeck et al. 2009; Luke et al. 2021) and modeling studies (Sotiropoulou et al. 2020; 2021b; Zhao et al. 2021; Zhao and Liu 2021; 2022) suggest that other SIP processes, like collisional break-up (Vardiman 1978; Takahashi et al. 1995) and drop-shattering (Lauber et al. 2018; Keinert et al. 2020), also have a significant influence on Arctic cloud microphysical structure.

In this study we implement descriptions for drop-shattering (DSH) and collisional break-up (BR) in NorESM2, using parameterizations from the recent literature (Phillips et al. 2017a,b; 2018). We further test the efficiency of sublimation break-up (SUBBR) (Oraltay and Hallett 1989; Bacon et al. 1998), a process whose efficiency remains unknown in real atmospheric conditions, using the parameterization developed by Deshmukh et al. (2022). In addition, we modify the existing HM description to further account for rain-snow collisions. Sensitivity simulations with varying PIP, SIP and ice aggregation treatment are conducted to quantify the ice-related processes that are most impactful on ice particle number. Results are initially evaluated against two-year surface-based observations from Ny-Ålesund for the period June 2016 - May 2018 to assess the most realistic simulation set-up. Satellite radiation and cloud measurements are further used to quantify the impact of the examined processes on the current climate state over the whole Arctic region.

2. Methods

a. Observations

Remote-sensing observations collected at Ny-Ålesund between June 2016–May 2018 are utilized to evaluate the model. Macro- and micro- physical cloud properties are derived from a combination of instruments that includes 94 GHz cloud radars, a ceilometer and a HATPRO radiometer (Nomokonova et al. 2019d). The Liquid water path (LWP) is derived from a HATPRO microwave radiometer (Nomokonova et al. 2019a,b,c), with typical uncertainty around +/- 20–25 g m^{-2}. Once the measured particles have been categorized as liquid droplets, ice, melting ice, and drizzle/rain using the Cloudnet retrieval algorithm (Illingworth et al. 2007), ice water content (IWC) is derived from radar reflectivity and temperature measurements following the methodology of Hogan et al. (2006). The uncertainties in this IWC retrieval range from -33% to +50% for temperatures above -20^{o}C and from -50% to +100% for temperatures below -40^{o}C. The effective radius of ice particles (r_{ieff}) is calculated following Delanoë and Hogan (2010), using IWC and visible extinction coefficient estimates (Ebell et al. 2020); the latter is also derived following Hogan et al. (2006). The uncertainty in r_{ieff} retrieval described by Delanoë and Hogan (2010) is about 30%, while the uncertainty for the radar-derived visible extinction coefficient that is used in the ice effective radii retrieval is 62% to 160% (Hogan et al. 2006). Thermodynamic variables such as temperature (Nomokovova et al. 2019d,e,f) and integrated water vapor (IWV; Nomokovova et al.

2019g,h,i) are also derived from HATPRO.

Surface in-situ cloud measurements were collected at the Zeppelin station with the Zeppelin Observatory counterflow virtual impactor (CVI) inlet (Karlsson et al. 2021a,b) for a similar period (until February 2018) as the remote sensing observations. However, this instrument samples only small cloud particles with diameters below 50 μm, thus it cannot be used for the evaluation of the whole modeled cloud particle spectrum. Finally, local measurements are complemented with satellite datasets to evaluate the modeled radiation and cloud properties over the whole Arctic region. These include the Clouds and Earth's Radiant Energy Systems (CERES; Wielicki et al. 1996) Energy Balanced and Filled (EBAF) product, edition 4.1 (Kato et al. 2018) and the GCM-Oriented CALIPSO Cloud Product (GOCCP) Version 3 (Chepfer et al. 2010).

b. Model description

For our investigations we use the NorESM2-MM version (Seland et al. 2020) with 1^{o} horizontal resolution. Wind and pressure fields are nudged every six hours towards ERA-Interim data (Dee et al. 2011) to limit the influence of meteorological errors on microphysical fields. Simulations are run for 29 months, from 1 January 2016 to 31 May 2018, with fixed sea-surface temperatures (SSTs). The Shared Socioeconomic Pathways 2 (SSP2) scenario is used which assumes emissions similar to the historical patterns. The first five months are considered as spin-up, while the rest of the output is used for comparison with surface-based observations from Ny-Ålesund. A description of the modeled ice microphysics, which is the main focus of this study, and the implemented modifications follows below.

The atmospheric component of NorESM2 is CAM6-Oslo, which consists of the Community Atmosphere Model version 6 (CAM6) and the OsloAero5.3 (Kirkevåg et al. 2018) aerosol scheme. CAM6-Oslo employs the Morrison and Gettelman (2015) microphysics scheme (MG2), which accounts for four hydrometeor types: cloud droplet, raindrop, cloud ice and snow. Heterogeneous PIP parameterizations follow the Classical Nucleation Theory (CNT; Hoose et al. 2010; Wang et al. 2014) which accounts for immersion, contact and deposition freezing of two INP types, dust and soot. Immersion freezing is only allowed to occur below -10^{o}C in this scheme for both INP species, while only 10% of the soot concentrations are considered efficient INPs. While CNT is the default nucleation scheme used for the CMIP6 simulations, the model employs an alternative option for PIP: CNT can be replaced by diagnostic parameterizations that are functions of basic thermodynamic variables and do not account for explicit cloud-aerosol interactions. These include the Bigg (1953), Young (1974) and Meyers et al. (1992) parameterizations for immersion, contact and deposition freezing, respectively. The Bigg (1953) and Young (1974) parameterizations are activated at temperatures below -4^{o}C, while Meyers et al. (1992) is active within the -37^{o}C–0^{o}C temperature range.

Secondary ice production is accounted in MG2 scheme only through the HM mechanism, which is parameterized following Cotton et al. (1998). This formulation considers a maximum splinter production of 350 splinters per milligram of rime at -5^{o}C, while the process efficiency decreases to zero at temperatures below (above) -8^{o}C (-3^{o}C). However, HM is only activated after cloud droplets collide with snow; in our modified code, we further account for the contribution from raindrop-snow collisions, using the same parameterization (Cotton et al. 1998) for the prediction of the generated fragments. Estimations of mass and number collision tendencies for raindrop-snow collisions are available in the standard MG2 scheme.

To represent the BR mechanism, we implement the parameterization of Phillips et al. (2017a). The process is initiated after snow particles collide with each other or with cloud ice. We assume that the collisions that do not instantaneously result in sticking (aggregation) are those that allow for particle bouncing and subsequent break-up. Phillips et al. (2017a) is a physically-based parameterization that predicts the number of generated fragments as a function of collisional kinetic energy (CKE), while the effect of the colliding particles' size, rimed fraction and ice habit is further accounted for. MG2 however does not predict the rimed fraction and ice habit. For this reason, we assume planar ice particles with a 0.4 rimed fraction in our simulations; planar shape encompasses a larger range of shapes and is valid for a wide temperature range, and a high rimed fraction has been shown to give the most optimal results in simulations of polar clouds (Sotiropoulou et al. 2020; 2021a). Furthermore, we limit BR activation at temperatures above -25^{o}C; this upper temperature limit is based on the recent findings of Pasquier et al. (2022), who found evidence of the BR process in Arctic observations collected at temperatures down to -24^{o}C. All generated fragments from this mechanism are added to the cloud ice category.

The DSH description follows Phillips et al. (2018) and is initiated after raindrop-INP (immersion freezing), raindrop-snow and raindrop-ice collisions. For ice multiplication due to raindrop-INP and raindrop-cloud ice collisions we utilize the formulation referred to as 'mode 1' in Phillips et al. (2018), which concerns the accretion of small particles by more massive raindrops, while for snow-raindrop the 'mode 2' formulation is applied. Mode 1 can generate both tiny and big fragments; the former are added to the cloud ice category, while the latter are considered to be snow. The new tiny fragments are assumed to have a fixed diameter of 10^{-5} m (Phillips et al. 2018) and a constant ice density of 500 kg m^{-3} (which is the default cloud ice density in the MG2 scheme), while the rest of the colliding rain mass is transferred to snow. Freezing probability in this mode is set to unity and zero, at temperatures below -6°C and above -3°C, respectively, while it takes intermediate values at temperatures between -6°C and -3°. Similarly, shattering probability is a function of raindrop size, set to 0 and 1 at sizes smaller than 50 μm and larger than 60 μm, respectively. Mode 2 can only generate tiny fragments. Tiny fragments are added to the cloud ice category, while big fragments are treated as snow.

Note that the MG2 scheme does not account for the accretion of cloud ice on raindrops. To estimate the number and mass collision tendencies for these interactions, we further implement the formulation proposed by Reisner et al. (1998), which is also utilized in the Morrison et al. (2005) microphysics scheme. Furthermore, to account for underestimations in CKE when the terminal velocity of the two colliding particles is similar ($u_1 \approx u_2$), we adapt the corrections in the mass- or number-weighted difference in terminal velocity (Δu_{12}) proposed by Mizuno (1990) and Reisner et al. (1998) in the bulk SIP implementations. When snowflakes collide with each other, it is assumed that 0.1% of the colliding mass is transferred to the generated fragments (Phillips et al. 2017a). The same assumption is applied to the mode 2 of the DSH process, thus only 0.1% of the colliding mass is transferred to the tiny fragments (Phillips et al. 2018). A detailed description of the implementation method can be found in Sotiropoulou et al. (2021a) and Georgakaki et al. (2022).

Deshmukh et al. (2022) recently developed an empirical formulation for sublimation break-up of graupel and dendritic snow, in which the total number of the ejected fragments (N) is proportional to the square root of the sublimated mass (M), $N = K \cdot M^{0.57}$, where K is a function of size (diameter) and relative humidity with respect to ice. Since graupel is not accounted for in the MG2 scheme, we apply this parameterization to sublimating snow and cloud ice, as long as the diameter for the latter exceeds 200 μm (note that the cloud-ice to snow autoconversion diameter is set to 500 μm in NorESM2). Sublimating cloud ice and snow mass is calculated by the default MG2 scheme. Moreover, since the Deshmukh et al. (2022) parameterization is developed based on the observations of dendritic particles, we only allow for sublimation break-up to activate between -10°C and -20°C, where such ice habits are more likely to occur (Bailey and Hallett 2009). All new fragments are added to the cloud-ice category. Sublimation break-up of graupel, which is expected to occur at all temperatures (Deshmukh et al. 2022), is not accounted in the model, since graupel is not treated in MG2.

Finally, while PIP and SIP are significant ice-crystal sources, aggregation is a critical sink that can substantially decrease the cloud-ice number. However, its parameterization is also a source of uncertainty in atmospheric models (Karrer et al. 2021). The MG2 scheme accounts for aggregation through cloud ice-snow and snow-snow collisions. Accretion of cloud ice by snow follows the "continuous collection" approach as described in Rutledge and Hobbs (1983), while snow-snow aggregation follows Passarelli (1978). The aggregation efficiency (E_{ii}) between ice particles is generally considered the product of their collision efficiency and sticking efficiency, with the latter depending on CKE and size (Phillips et al. 2015). However, a very simplified approach for E_{ii} is usually found in climate models; in CAM6-Oslo this parameter is set constant to 0.5 (while it was 0.1 in the previous model version).

c. Sensitivity simulations

In this study, we examine the sensitivity of Arctic clouds to three main processes that determine cloud ice number: PIP, SIP and ice aggregation. At this point, it is worth noting that a bug has been recently identified in MG2 (Shaw et al. 2021), which limits ice formation in mixed-phase clouds. This is due to an upper limit (n_{imax}) imposed for the ICNCs, that is equal to the INP number. Neither heterogeneous freezing processes nor SIP contribute to this INP limit, preventing them from producing new ice crystals (Shaw et al. 2021). In all our simulations we remove this n_{imax} limit, allowing PIP and SIP to evolve prognostically in the stratocumulus clouds. Our investigations on PIP effects include the use of either the prognostic or the diagnostic treatment for the freezing processes (see section 2*b*). Simulations that employ the Hoose and Möhler (2012) parameterization include the abbreviation 'CNT' in their name, while the ones that are run with diagnostic descriptions (Meyers et al. 1992; Bigg 1953; Young et al. 1974) include the prefix 'MBY' (Table 1).

Sensitivity to SIP descriptions is examined by (a) either accounting for the standard SIP treatment in CAM6-Oslo which includes only the HM process after cloud droplet - snow collisions or (b) activating all the additional mechanisms, described in section 2*b*, simultaneously. Moreover, the performance of SIP processes like BR and DSH, which are a function of CKE, can be sensitive to different implementation methods. In this study, we examine the performance of bulk vs hybrid-bin descriptions of SIP. Our bulk implementations follow the methodology of Sotiropoulou et al. (2020; 2021a,b) and Georgakaki et al. (2022) for BR and DSH, respectively. In their studies, the characteristic diameters and number-weighted velocities for each hydrometeor are used as input parameters for the Phillips et al. (2017a) and (2018) schemes, while the standard MG2 formulations for accretion/aggregation rates are used to estimate the collisions that lead to SIP.

A different approach was adapted by Zhao et al. (2020), who used an emulated bin approach to parameterize the two mechanisms described above, which better accounts for the impact of the size spectra variability on the collision rates and collisional kinetic energy. In their framework, the collision rates are calculated for each bin as $E_c\, \delta N_1\, \delta N_2\, \pi\, (r_1+r_2)^2\, |u_1-u_2|$, where E_c is the collision efficiency, and δN_1 and δN_2 are the number concentrations in the two bins with particle radii r_1 and r_2, respectively. Similar to the bulk approach, the number of generated fragments per collision is estimated following Phillips et al. (2017a, 2018). Each new fragment produced by these two processes is assumed to have a 10-μm size (Phillips et al. 2018). Sensitivity simulations that account for all SIP mechanisms include the abbreviation 'SIP' in their name (Table I). If an emulated bin framework is used instead of a bulk description, this suffix is modified to 'SIPBN'. Note that the emulated bin framework is only tested for BR and DSH; a bulk approach is always used for HM and sublimation break-up in the model.

A previous application of these parameterizations in Arctic conditions (Sotiropoulou et al. 2020) has shown that BR is the dominant SIP mechanism. However, Sotiropoulou et al. (2021b) showed that the Phillips et al. (2017a) parameterization is largely sensitive to the sublimation factor (ψ) – a correction factor for ice enhancement due to sublimation included in the BR formulation (see Appendix A). This factor was induced to account for the fact that the field data (Vardiman, 1978) used to constrain the number of fragments generated by this process were not collected in realistic in-cloud conditions. Dr. Vaughan Phillips suggests that the prescribed ψ in Phillips et al. (2017a) study is overestimated, leading to underestimation of the BR efficiency. For this reason we perform two more sensitivity simulations, with both prognostic and diagnostic PIP, with this factor removed from the BR formulation. These experiments include the suffix 'SIPBNψ' in their name, as they are combined with the more advanced emulated bin framework.

Finally, ice aggregation is another process that has a significant impact on ICNCs, but its efficiency is described through a tuning parameter (E_{ii}) in the model. Generally, observations from mid-latitudes indicate the presence of two temperature zones that promote aggregation: one around -15°C (Barret et al. 2019) associated with enhanced dendritic growth that facilitates interlocking of the ice crystal branches (Connoly et al. 2012), and a second one close to the melting layer (Lamb and Verlinde 2011), caused by the increased sticking efficiency of melting snowflakes. However, an analysis of recent dual-wavelength radar observations of shallow clouds from Ny-Ålesund suggests that enhanced aggregation occurs mostly between -10^{o}C and -15^{o}C (Chellini et al. 2021), while no evidence of this process is found at higher temperatures. To adjust the aggregation efficiency to these new findings we perform simulations with a modified E_{ii}. In the standard scheme, E_{ii} remains constant at 0.5 throughout the whole temperature range, while in our sensitivity simulations with the suffix 'AGG' this high value is only sustained between -10^{o}C and -15^{o}C. At colder temperatures, E_{ii} is set to 0.1, while at warmer temperatures aggregation is deactivated (E_{ii}=0). A summary of all the performed sensitivity tests and the different combinations of PIP, SIP and aggregation treatments is given in Table 1.

TABLE 1: Description of the sensitivity simulations

	Primary Ice Production	Secondary Ice Production	Aggregation
CNT (CONTROL)	prognostic (CNT)	HM (cloud droplet-snow)	constant E_{ii}
MBY	diagnostic (Meyers et al., Bigg , Young)	HM (cloud droplet-snow)	constant E_{ii}
CNT_AGG	prognostic (CNT)	HM (cloud droplet-snow)	variable E_{ii}
MBY_AGG	diagnostic (Meyers et al., Bigg, Young)	HM (cloud droplet-snow)	variable E_{ii}
CNT_SIP	prognostic (CNT)	HM (cloud droplet/rain-snow), bulk BR, bulk DS, SUBBR	constant E_{ii}
MBY_SIP	diagnostic (Meyers et al., Bigg, Young)	HM (cloud droplet/rain-snow), bulk BR, bulk DS, SUBBR	constant E_{ii}
CNT_SIPBN	prognostic (CNT)	HM (cloud droplet/rain-snow), bin BR, bin DS, SUBBR	constant E_{ii}
MBY_SIPBN	diagnostic (Meyers et al., Bigg, Young)	HM (cloud droplet/rain-snow), bin BR, bin DS, SUBBR	constant E_{ii}
CNT_SIPBNψ	prognostic (CNT)	HM (cloud droplet/rain-snow), bin BR (ψ=1), bin DS, SUBBR	variable E_{ii}
MBY_SIPBNψ	diagnostic (Meyers et al., Bigg, Young)	HM (cloud droplet/rain-snow), bin BR (ψ=1), bin DS, SUBBR	variable E_{ii}
CNT_SIPBN_AGG	prognostic (CNT)	HM (cloud droplet/rain-snow), bin BR, bin DS, SUBBR	variable E_{ii}

MBY_SIPBN_AGG	diagnostic (Meyers et al., Bigg, Young)	HM (cloud droplet/rain-snow), bin BR, bin DS, SUBBR	variable E_{ii}
CNT_SIPBNψ_AGG	prognostic (CNT)	HM (cloud droplet/rain-snow), bin BR (ψ=1), bin DS, SUBBR	variable E_{ii}
MBY_SIPBNψ_AGG	diagnostic (Meyers et al., Bigg, Young)	HM (cloud droplet/rain-snow), bin BR (ψ=1), bin DS, SUBBR	variable E_{ii}

3. Results

a. Ny-Ålesund site

1) Cloud properties

In this section we focus on the evaluation of the simulated cloud macrophysical properties against remote-sensing surface observations collected at Ny-Ålesund (see section 2*a*). An evaluation of the modeled thermodynamic conditions is presented in Figs. S1 and S2 in the Supporting Information. NorESM2 is in reasonably good agreement with temperature (Fig. S1) and IWV (Fig. S2) measurements, although somewhat colder conditions are often found in the model within the lowest first kilometer of the atmosphere (Fig. S1).

Instantaneous modeled ICNC and IWC values derived at 3-hour time resolution are used in Fig. 1, which presents the interquartile range and median estimates as a function of temperature. IWC retrievals are averaged over a ±10-minute window around the model output timesteps and within ±20 meters around the model vertical levels, while ICNC measurements are not available at this site.

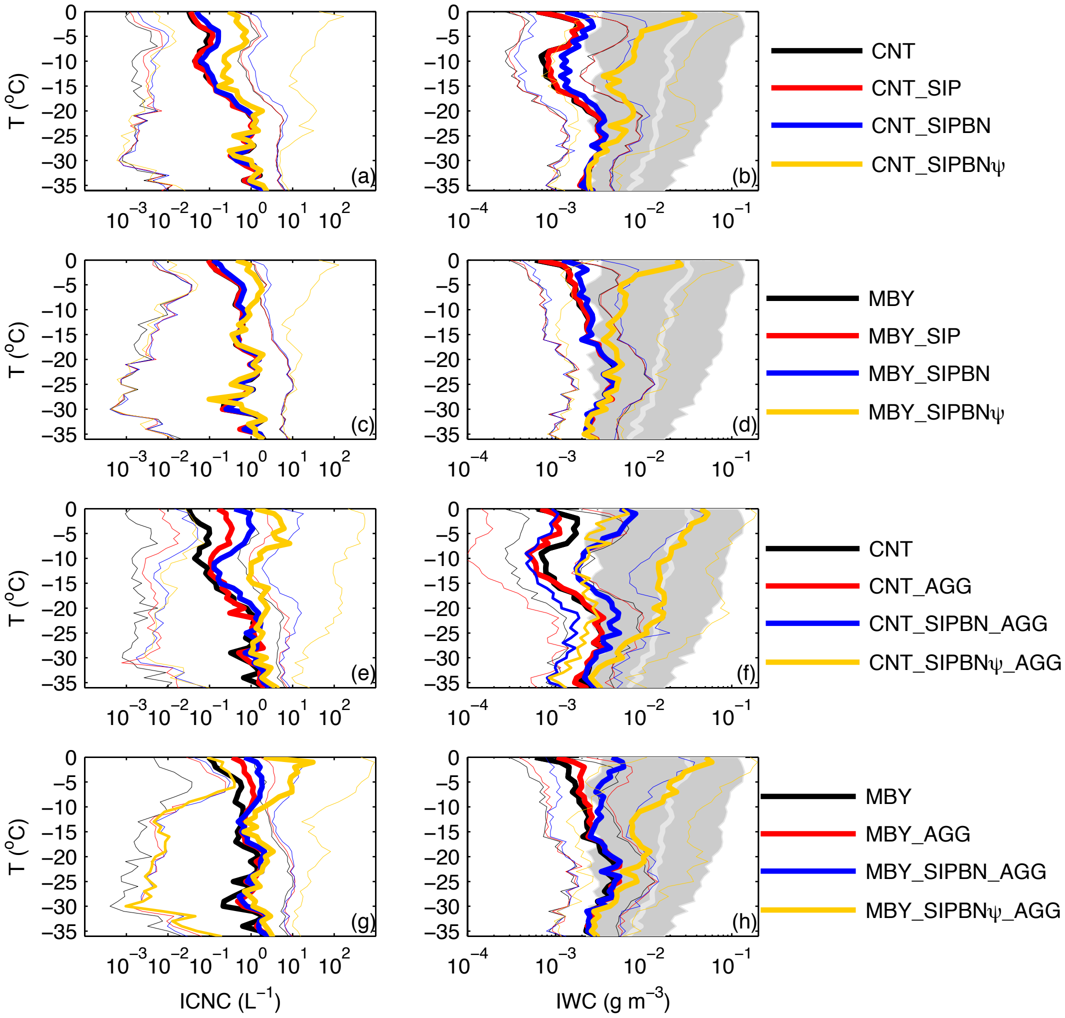

FIG 1. (a, c, e, g) Ice crystal number concentration (ICNC) and (b, d, f, h) ice water content (IWC) as a function of temperature. Thick (thin) lines indicate median values (25^{th} and 75^{th} percentiles). Grey shading (line) shows the observed interquartile range (median). Results are derived from the Ny-Ålesund site (gridpoint) for the period June 2016- May 2018. The observed IWC values are averaged over a ±10-minute window around the model output timesteps and within ±20 meters round the model vertical levels.

The aerosol-aware CNT (control) simulation produces median ICNC concentrations slightly below 0.1 L^{-1} within the 0°C to -15°C temperature range (Fig. 1a), which results in a median IWC that is more than one order of magnitude lower than the observed (Fig. 1b). The CNT interquartile range of IWC barely overlaps with the observed in Fig. 1b, while the discrepancies between model and observations are reduced below -20°C: the median IWC in the CNT simulation is about a factor of 5 lower than the observed at these cold temperatures. There is hardly any difference in ice properties between CNT and CNT_SIP simulations (Fig. 1a,b), while CNT_SIPBN results in very weak ICNC and IWC enhancement compared to CNT (about 50% in the median values) at temperatures above -20°C. CNT_SIPBNψ is the only simulation that results in significant ICNC enhancement, resulting in 5-10 times larger median values (Fig. 1a) at the relatively warm temperatures compared to CNT. CNT_SIPBNψ is the simulation that best agrees with IWC observations in Fig. 1b, as it is the only set-up that produces median IWC values that fall within the observed interquartile range.

The MBY simulation (Fig. 1c, d) produces about 3-10 times higher median ICNCs than CNT at temperatures above -15^{o}C, which improves the median IWC by a factor of 2-3. Improvements at colder temperatures are minor with the diagnostic PIP treatment. MBY_SIP gives similar results to the MBY simulation, while MBY_SIPBN results in a very weak shift of the ICNC and IWC interquartile range towards larger values. Again, MBY_SIPBNψ, the simulation with the modified BR description (see Table 1), is the only one that results in a pronounced ICNC enhancement (Fig. 1c), which results in a more realistic IWC representation (Fig. 1d) compared to MBY, MBY_SIP and MBY_SIPBN. The results in panels (a-d) suggest that the bulk implementation of the BR and DSH mechanisms in the MG2 scheme limits their efficiency, compared to the use of a hybrid-bin framework. However, the treatment of the sublimation factor ψ in the BR parameterization is even more critical for the efficiency of this process, as CNT_SIPBNψ (MBY_SIPBNψ) produces on average 5(4) times larger IWC values than CNT_SIPBN (MBY_SIPBN) at the temperature range where the BR process is active.

Panels (e-h) aim to examine the impact of reduced aggregation on both PIP and SIP efficiency. CNT_AGG (Fig. 1e) results in a ~4-fold ICNC enhancement at temperatures above -15^{o}C, which is accompanied by a shift of the 25th IWC percentile towards smaller values, increasing the discrepancy from the observations (Fig. 1f). This is likely because decreased aggregation increases the number of ice crystals, but at the same time it decreases their size and thus their efficiency in the WBF process. CNT_SIPBN_AGG shifts the ICNC interquartile range at on average 10 times higher values (Fig. 1e) within the warm subzero temperature range, which results in IWC values that are in better agreement with observations (Fig. 1f). This simulation produces a median IWC within the observed interquartile range. The fact that the CNT_SIPBN_AGG simulation is much more efficient in ICNC enhancement than both CNT_SIPBN (Fig. 1a) and CNT_AGG indicates an important interplay between SIP and ice aggregation. An overestimated aggregation rate can substantially limit ice multiplication, as the new fragments will rapidly aggregate and form precipitation-sized particles that will lead to IWC depletion through sedimentation. It is worth noting that the worst CNT_SIPBN_AGG performance is found at temperatures between -10^{o}C and -25^{o}C, where the default aggregation efficiency remains unaffected (see section 2*c*). This suggests that constraining ice aggregation is critical for the representation of Arctic cloud properties, especially in conditions that favor SIP.

Finally, the CNT_SIPBNψ_AGG simulation, that combines a more efficient BR mechanism with decreased aggregation, is the only set-up that results in up to two orders of magnitude larger median ICNC values compared to CNT (Fig. 1e) and produces an IWC interquartile range that is very similar to the observed (Fig. 1f). The simulations with the diagnostic PIP scheme in Figs. 1g and 1h respond to aggregation and BR modifications in a similar way as the CNT simulations discussed above, suggesting that results are less sensitive to PIP than to SIP and aggregation treatment.

Unfortunately, the modeled ICNCs presented in Fig. 1 cannot be evaluated against observations, as no such measurements were performed at Ny-Ålesund during the examined period. Only measured cloud particle concentrations over a limited size range (5-50 μm) collected with a CVI are available (see section 2*a*). These are shown in Fig. 2 along with the modeled droplet and cloud ice size spectra that include the measured size range. Size spectra of larger particles, rain and snow, are also shown in the same figure to give a complete overview of the microphysical differences between the different simulations.

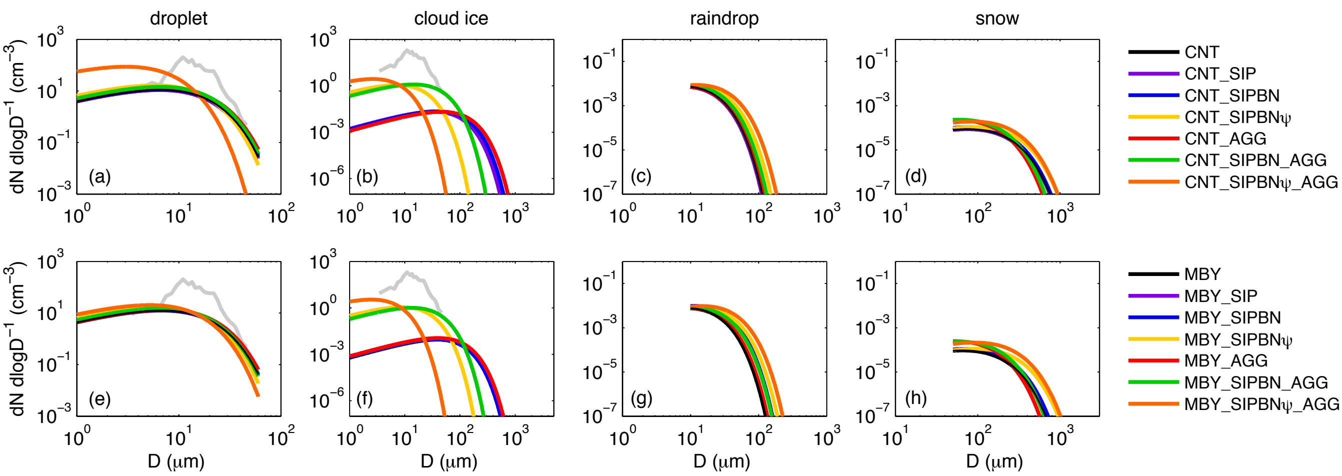

FIG 2. (a, e) droplet, (b, f) cloud ice, (c, g) raindrop and (d, h) snow size distributions for the different model sensitivity simulations. The first (second) row of panels presents simulations conducted with prognostic (diagnostic) PIP. Grey lines in panels (a, e) and (b, f) represent the observed spectrum derived from CVI for the size range 5-50 μm. All data span the period June 2015 - February 2018, as CVI measurements were not collected beyond this date.

All model simulations underestimate the hydrometeor concentrations measured by the CVI. CNT_SIPBN_AGG (Fig. 2b) and MBY_SIPBN_AGG (Fig. 2f) result in a pronounced shift of the cloud ice spectra towards smaller sizes (Fig. 2b, f), which somewhat improves agreement with observations within the measured size range. Same behavior is found in CNT_SIPBNψ (Fig. 2b) and MBY_SIPBNψ (Fig. 2f) simulations, however these two experiments also produce a weak shift of the precipitation particle spectrum to larger sizes (Fig. 2d, e, g, h). CNT_SIPBNψ_AGG and MBY_SIPBNψ_AGG (Fig. 2a) produce the most pronounced differences in particles' spectra than all simulations. CNT_SIPBNψ_AGG substantially enhances the concentration of droplets between 1-10 μm, while this enhancement is much weaker in MBY_SIPBNψ_AGG (Fig. 2e). Both these simulations produce large concentrations of cloud ice particles between 1-10μm, but no cloud ice at sizes above 50 μm (Fig. 2b, f). However, raindrop and snow concentrations at these sizes are clearly enhanced compared to the other simulations (Fig. 2d, e, g, h). A comparison of the cloud ice and snow spectra reveals that the large ICNC enhancements observed in Fig. 1 for simulations with effective SIP mainly occur through an enhancement of the cloud ice category.

Apart from the CVI observations, insights into the microphysical properties can be obtained from the radar-retrieved r_{ieff}. However, this dataset is associated with large uncertainties (see section 2*a*). The retrievals result in a median (75^{th} percentile) r_{ieff} of 49 μm (52 μm). These values are 76 μm (121 μm) for CNT and 84 μm (126 μm) for MBY, while somewhat improved r_{ieff} statistics are obtained for CNT_SIPBN_AGG, 71 μm (107 μm), and MBY_SIPBN_AGG, 75 μm (113 μm). Further decreased radii are produced by CNT_SIPBNψ and MBY_SIPBNψ, respectively: 63 μm (90 μm) and 66 μm (97 μm). The best agreement with the retrieved r_{ieff} statistics is achieved by CNT_SIPBNψ_AGG, 56 μm (77 μm) and MBY_SIPBNψ_AGG, 58 μm (82 μm). All the other simulations give similar r_{ieff} values to CNT and MBY. Despite the uncertainty in the radar estimates, the overall small radii suggest very limited aggregation and is indicative of SIP occurrence.

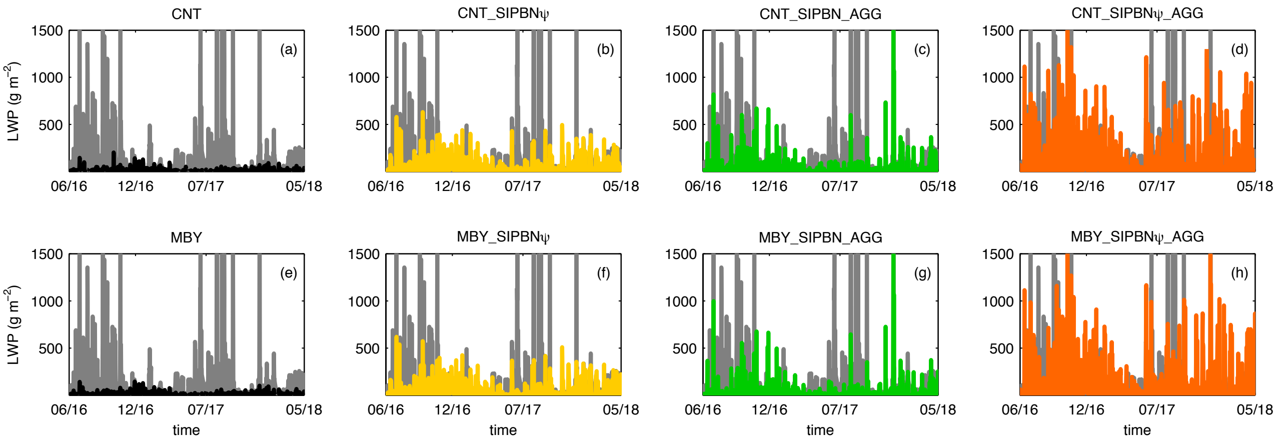

FIG 3. Timeseries of liquid water path (LWP) for the different model sensitivity simulations. The first (second) row of panels presents simulations conducted with prognostic (diagnostic) PIP. Grey lines in all panels represent radiometer measurements.

The representation of the cloud liquid phase is evaluated using radiometer measurements of LWP, interpolated at the model timesteps (Fig. 3, Table 2). Figure 3 shows the sensitivity simulations that result in the most pronounced differences compared to CNT and MBY. Median and mean LWP statistics for all simulations are shown in Table 2. CNT and MBY substantially underestimate LWP, especially during the warm seasons (Fig. 3a, e). The modeled median LWP agrees with the observed value, however, the mean LWP values are underestimated by a factor of ~6. Modifying aggregation, as in the CNT_AGG and MBY_AGG simulations, somewhat improves the LWP statistics (Table 2), however, the mean LWP remains about ~5 times underestimated. The simulations characterized by very weak SIP efficiency in Fig. 1 (CNT_SIP, CNT_SIPBN, MBY_SIP, MBY_SIPBN) result in even more underestimated LWP values (Table 2).

A mean LWP larger than 30 g m^{-2} (Table 2), which is indicative of the dominance of optically-thick clouds (Stephens 1978) is only produced by the simulations with substantially enhanced ice production (yellow lines in Fig. 1) compared to the standard model set-up. These are the only simulations that produce LWP values comparable to observations (Fig. 3). Note that LWP measurements indicate a positively skewed distribution with a mean LWP about ten times higher than the median value (Table 2). A similar distribution shape is only produced by CNT_SIPBNψ, MBY_SIPBNψ, CNT_SIPBN_AGG and MBY_SIPBN_AGG, CNT_SIPBNψ_AGG and MBY_SIPBNψ_AGG, which result in a median LWP value about 6-8 times lower than the mean. However, CNT_SIPBNψ_AGG and MBY_SIPBNψ_AGG are the two simulations that produce the more realistic LWP statistics; their deviation from the observed mean/median LWP falls within the instrument's uncertainty range ~25 g m^{-2} (Table 2). These are also the simulations that produce the largest LWP values (Fig. 2d, h), while at the same time they are characterized by the highest IWC (Fig. 1). The enhanced liquid content is consistent with the generally higher cloud and rain droplet concentrations found in Fig. 2 for these simulations. Yet, the positive correlation between liquid and ice enhancement seems paradoxical, as increasing ice production is usually associated with liquid depletion in mixed-phase clouds.

TABLE 2: Median and mean Liquid Water Path (LWP) for all sensitivity simulations.

Simulations	Median LWP (g m^{-2})	Mean LWP (g m^{-2})
Observations	9.4	94.0
CNT (CONTROL)	9.0	16.0
MBY	8.3	15.7
CNT_AGG	9.9	20.5
MBY_AGG	9.0	18.8
CNT_SIP	2.8	10.3
MBY_SIP	4.2	11.5
CNT_SIPBN	2.9	12.4
MBY_SIPBN	4.4	12.9
CNT_SIPBNψ	7.1	44.0
MBY_SIPBNψ	6.9	40.6
CNT_SIPBN_AGG	4.7	34.8
MBY_SIPBN_AGG	5.3	33.1
CNT_SIPBNψ_AGG	17.3	110.4
MBY_SIPBNψ_AGG	13.3	103.9

2) Microphysical processes

To better understand the interactions between the underlying microphysical processes that drive the macrophysical differences between the different sensitivity simulations, vertical profiles of mean PIP, SIP, WBF and riming tendencies are plotted in Fig. 4. The ice multiplication tendencies of the individual SIP mechanisms are shown in Fig. 5. Interestingly, when a diagnostic PIP treatment is applied (Fig. 4e), PIP rates generally decrease with increasing ice production through modifications in SIP and/or aggregation, a behavior that is not found in simulations with CNT (Fig. 4a). An analysis of the changes in thermodynamic profiles between the simulations (Fig. S3a, c) indicate warmer temperatures with increasing ice production, especially at heights above 1 km, while the specific humidity response is more variable (Fig. S3b, d); since the diagnostic PIP parameterizations are solely dependent on the thermodynamic conditions, these temperature variations can explain to a large extent the variable PIP rates in Fig. 4e. In Fig. 4a substantial differences in PIP are only found for CNT_SIPBNψ and CNT_SIPBNψ_AGG; these differences seem to follow changes in specific humidity profiles (Fig. S3b, d) suggesting that the prognostic PIP treatment is mostly affected by variations in supersaturation.

SIP rates in CNT_SIP and MBY_SIP are very similar to CNT and MBY (Fig. 4b, f). This is in agreement with the findings of Fig. 1, which reveal that the bulk implementations of BR and DSH hardly result in any ice multiplication. This result is further confirmed by Fig. 5 which shows that BR and DSH tendencies are orders of magnitude smaller than those of HM. Another interesting finding is that including rain-snow collisions in the HM description in the CNT_SIP and MBY_SIP simulations does not enhance the efficiency of this process compared to CNT and MBY that account only for cloud drop-snow collisions (Fig. 5a, e), as the precipitation particle concentrations are generally limited (Fig. 2c,d,g,h). Furthermore, sublimation breakup activates in the lowest five atmospheric kilometers, but remains extremely weak through the whole layer (Fig. 5d, h).

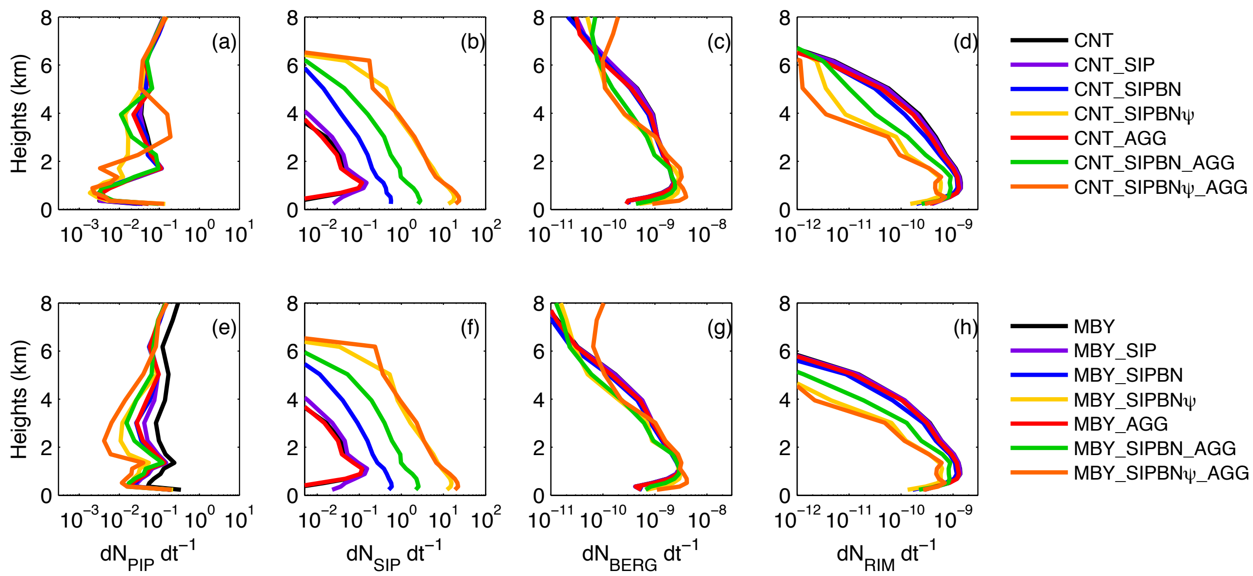

FIG 4. Mean vertical profiles of number concentration tendencies (kg^{-1} s^{-1}) due to (a, e) PIP and (b, f) SIP, (c, g), and mass concentration tendencies (kg kg^{-1} s^{-1}) due to WBF and (d, h) riming for the different model sensitivity simulations. The WBF rate is the sum of the individual rates for cloud ice and snow particles, while riming is the sum of cloud droplet and rain accretion on snow. The first (second) raw of panels presents simulations conducted with prognostic (diagnostic) PIP.

Utilizing an emulated bin framework for BR and DSH enhances SIP rates by on average a factor of ~5 in the lowest 4 atmospheric kilometers, compared to the simulations that adapt bulk frameworks (Fig. 4b, f). SIP also becomes prominent at higher altitudes (> 4 km), where bulk parameterizations do not produce any ice multiplication. Figure 5 indicates that the SIP is mainly due to the BR process. Although the emulated bin framework enhances DSH efficiency, the DSH rates remain substantially lower than those that correspond to the BR mechanism. Decreasing aggregation in CNT_SIPBN_AGG and MBY_SIPBN_AGG increases SIP efficiency by on average a factor of 5 (Fig. 4b, f), compared to CNT_SIPBN and MBY_SIPBN simulations, mainly through the enhancement of the BR process (Fig. 5b, f). Interestingly, the largest sensitivity of SIP is found in the treatment of the sublimation correction factor ψ in BR description. The simulations with ψ=1 (Table 1), that do not account for this correction result in BR rates enhanced by 1-1.5 orders of magnitude (Fig. 5b,f), which highlights the importance of constraining this parameter for an accurate BR representation. It is worth noting that increasing BR efficiency is associated with decreasing HM rates (Fig. 5). This is due to the fact that increasing SIP results in smaller ice particle sizes that are less likely to rime and initiate HM. The impact of SIP on riming and the WBF efficiency will be discussed below.

The simulations with a modified ψ factor and/or aggregation efficiency are characterized by an enhanced (reduced) WBF efficiency in the low-level (mid-level) clouds (Fig. 4c, g) compared to the rest of the simulations that produce significantly less ice content (Fig. 1). These simulations are also characterized by decreased riming efficiency throughout the whole troposphere (Fig. 4d, h). This is likely due to the shift of the frozen hydrometeor spectra to smaller particle sizes (Fig. 2) that are less efficient in depositional growth and liquid accretion. These interactions can explain why the simulations with the largest ice multiplication are at the same time the ones characterized by the highest LWPs (Fig. 3).

Our findings indicate that the inclusion of missing SIP mechanisms in NorESM2 can improve the macrophysical representation of Arctic mixed-phase clouds, but this requires the use of an emulated bin framework for BR and DSH, which is computationally about two times more demanding than the bulk descriptions of SIP. Modifications in the HM description, with the inclusion of rain-snow interactions, did not enhance the efficiency of this process in the examined conditions, suggesting that these modifications are redundant. BR appears to be the dominant SIP mechanism, however its efficiency is very sensitive to the treatment of the poorly constrained parameter ψ. DSH and SUBR processes are substantially weaker in the examined conditions. DSH is likely not favored due to lack of relatively large drops to initiate the process (Fig. 2c, g), while SUBBR is likely limited by the high relative humidity conditions that generally dominate in the Arctic.

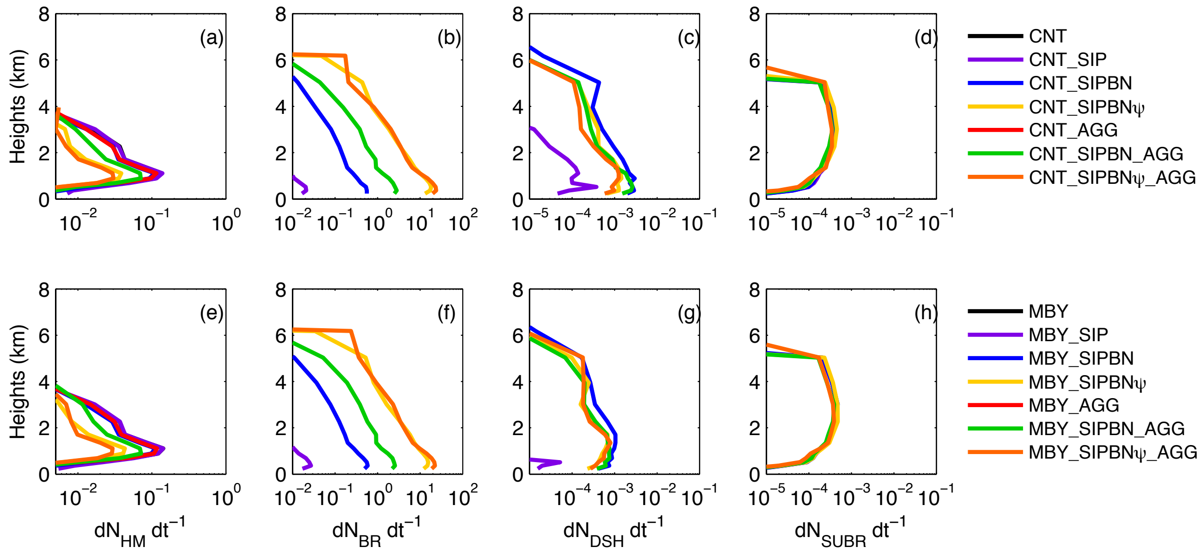

FIG 5. Mean vertical profiles of number concentration tendencies (kg^{-1} s^{-1}) due to SIP from the (a, d) HM, (b, f) BR and (c, f) DSH and (d, h) SUBBR for the different model sensitivity simulations. The first (second) row of panels presents simulations conducted with prognostic (diagnostic) PIP.

b. Arctic region

In this section, the performed simulations are evaluated against satellite observations averaged over the whole Arctic region (>66°N). The only simulations that are not included in this section are CNT_SIP and MBY_SIP, since the underlying microphysical processes (Figs. 4, 5) are very similar to CNT and MBY, respectively. Figure 6 shows the simulated radiation biases compared to EBAF v4.1 measurements (see section 2.1). We focus on the downward surface radiation components, longwave (LWD), shortwave (SWD) and their sum (TWD), which are directly influenced by clouds. The upward components are largely determined by the surface conditions.

The model underestimates the surface LWD by ~20 W m^{-2} from the late autumn to spring season when using the CNT PIP scheme (Fig. 6a), and the bias is somewhat larger with the diagnostic primary ice treatment (Fig. 6d). A similar LWD overestimation (~17 W m^{-2}) occurs in summer, but it does not vary with different PIP treatments. This suggests that the summer LWD bias is mainly linked to warm cloud processes (Shaw et al. 2021). The only simulations that significantly improve the representation of the LWD component are CNT_SIPBNψ_AGG and MY_SIPBNψ_AGG, which decrease the LWD bias by up to ~7.5 W m^{-2} during the cold months.

The SWD component is underestimated in the summer by NorESM2, with SWD biases reaching a maximum of -36 and -25 W m^{-2}, respectively, in the standard CNT and MBY simulations (Fig. 6b, e). On contrary, SWD is overestimated in late spring, with the bias being larger in simulations with a diagnostic PIP. CNT_SIPBNψ_AGG overall enhances these biases, degrading the representation of the incoming solar radiation (Fig. 6b). MBY_SIPBNψ_AGG results in larger SWD biases in the summer months compared to MBY, but improves the SWD representation in April and May (Fig. 6e). The rest of the simulations do not differ significantly from the standard NorESM2 version (CNT or MBY).

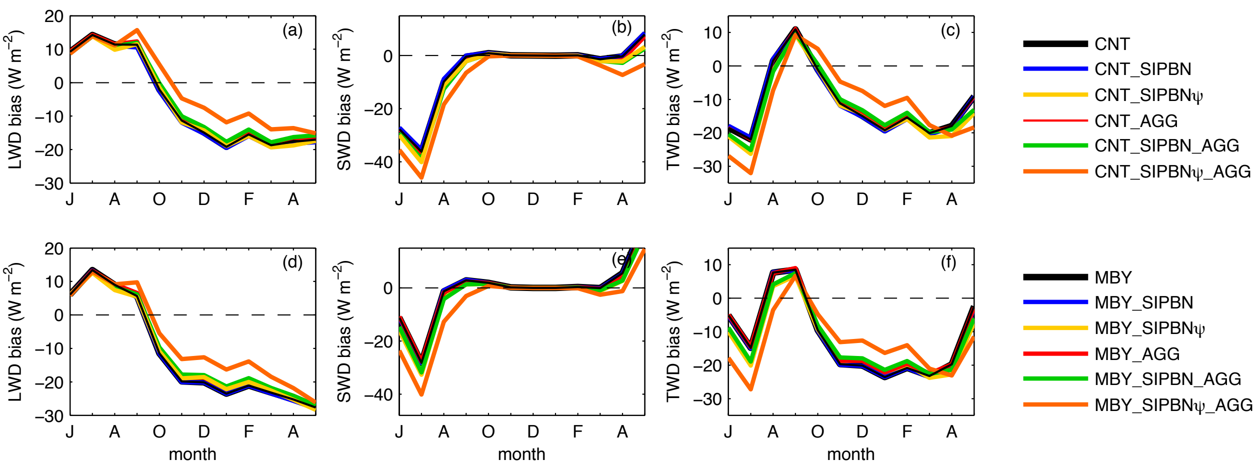

FIG 6. Timeseries of mean monthly surface downward (a, d) longwave, (b, e) shortwave and (c, f) total radiation biases (model – EBAF) for different NorESM2 sensitivity simulations. The first (second) row of panels presents simulations conducted with prognostic (diagnostic) PIP. Data are averaged over the whole Arctic region, above 66^{o}N, for the period June 2016-May 2018.

When adding the two radiation components, (Fig. 6c, f) NorESM2 results in negative TWD biases from mid-autumn to early summer (October-June), while a positive bias is found in August-September. The CNT_SIPBNψ_AGG and MBY_SIPBNψ_AGG produce reduced TWD biases in the dark months, from October to March, as TWD is dominated by LWD during this period. However, these simulations result in worse agreement with EBAF measurements compared to CNT and MBY between May-July, when the SWD component becomes more important.

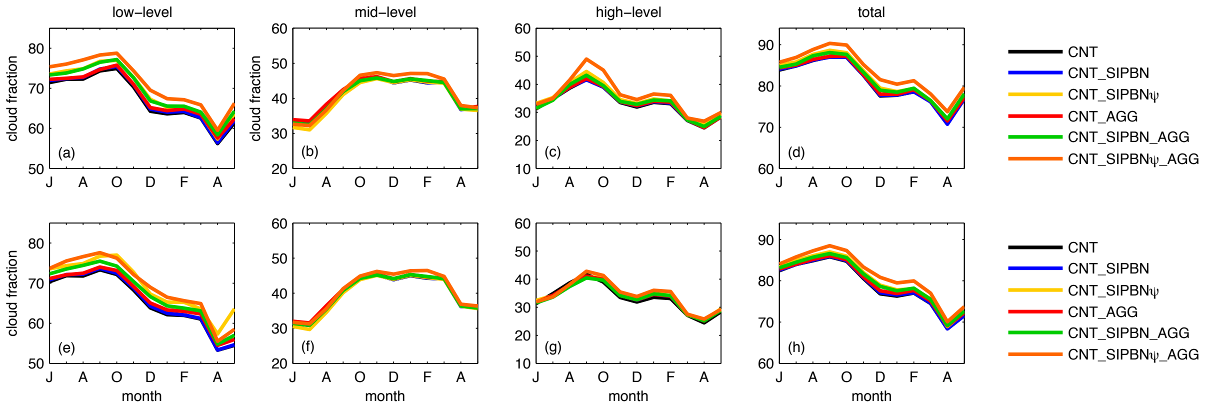

FIG 7. Timeseries of mean monthly (a, e) low-, (b, f) mid-, high- (c, g) and (d, h) cloud cover (model for the different NorESM2 sensitivity simulations. All data are vertically integrated over each model grid. The first (second) raw of panels presents simulations conducted with prognostic (diagnostic) PIP. Data are averaged between 66^{o}N and 82^{o}N for the period June 2016-May 2018.

The modeled cloud fraction is shown in Fig. 7. For a more subjective evaluation against the GOCCP satellite product, a modified cloud fraction derived from the Cloud feedback model intercomparison Observations Simulator package (COSP) is shown in Fig. S4. The CNT_SIPBNψ_AGG and MBY_SIPBNψ_AGG simulations with the largest ice production, result in enhanced low-level cloud cover during the whole year (Fig. 7a, e), compared to the rest of the sensitivity experiments. A weak enhancement is also found in mid-level cloud cover during the cold months in these two simulations. High-level cloud cover is larger in CNT_SIPBNψ_AGG compared to the rest of the simulations shown in Fig. 7c, especially in August-October, while no significant differentiations are found in simulations with a diagnostic PIP (Fig. 7g). These results are generally consistent with the behavior of LWD in Fig. 6, as the larger low-level cloud fraction in the CNT_SIPBNψ_AGG and MBY_SIPBNψ_AGG simulations result in enhanced downward longwave emission. Total cloud cover is also higher in these two experiments (Fig. 7d, h), while weak increases are also found in CNT_SIPBNψ, MBY_SIPBNψ, CNT_SIPBNψ_AGG and MBY_SIPBNψ_AGG, compared to the rest of the simulations. The COSP-derived results (Fig. S4) produce a more enhanced mid-level and high-level cloud response to increasing ice formation, compared to the standard model output (Fig. 7). Overall, COSP total cloud fraction somewhat increases in

CNT_SIPBNψ_AGG and MBY_SIPBNψ_AGG compared to CNT and MBY, respectively, resulting in a slightly improved agreement with the GOCCP observations during the dark months (Fig. S4).

4. Summary

In this study, we examine the sensitivity of Arctic cloud properties to the representation of ice microphysical processes in NorESM2. The primary target is to quantify the impact of PIP and SIP parameterizations on the cloud macrophysical structure and radiative effects. Sensitivity simulations with PIP are performed with two different primary ice treatments: (a) a prognostic CNT scheme that explicitly predicts ice formation from cloud-aerosol interactions and (b) diagnostic temperature-dependent parameterizations for all the heterogeneous freezing processes. The standard version of NorESM2 accounts only for the HM process through droplet-snow collisions. The sensitivity to SIP is examined by implementing additional SIP mechanisms, namely the BR, DSH and SUBBR mechanisms. Furthermore, the HM description is modified to account for rain-snow collisions.

The interactions of PIP and SIP with ice aggregation are also a subject of the present study. The standard parameterization of this process in NorESM2 includes a constant aggregation efficiency (E_{ii}) set to 0.5. To investigate the sensitivity of our results to this parameter, we adapt a variable E_{ii} which is qualitatively constrained by recent dual-wavelength radar measurements of shallow Arctic clouds (Chellini et al. 2021): E_{ii} is set to 0.5 at temperatures between -10^{o}C and -15^{o}C and to 0 (0.1) at temperatures below (above) this range. The model results are evaluated against surface observations from Ny-Ålesund and satellite retrievals over the whole Arctic.

Using CNT instead of diagnostic PIP descriptions results in a worse agreement with IWC observations from Ny-Ålesund at temperatures between -5^{o}C and -15^{o}C, when no other modification in SIP or aggregation is implemented. We speculate that the reason for this behavior is that the NorESM2 CNT parameterization does not account for aerosol types that are efficient INPs at relatively warm temperatures (e.g. biological aerosols). The additional SIP mechanisms enhance ice production, but BR and DSH mechanisms are efficient only when an emulated bin framework is used for their description. While bulk descriptions of these mechanisms are efficient in polar conditions in higher-resolution models (Sotiropoulou et al. 2020; 2021b), they hardly lead to any ice multiplication in NorESM2. We speculate that this happens for two main reasons. First of all, BR efficiency depends highly on the number and type of frozen hydrometeors. The MG2 scheme accounts only for two frozen categories, cloud ice and snow, thus only two types of collisions can lead to break-up: cloud ice-snow and snow-snow. Other schemes that account for graupel or hail (e.g. Morrison et al. 2005) can describe BR from a substantially larger number of collision types and may result in more efficient SIP. Moreover, using the characteristic diameter of each hydrometeor category as input to the BR and DSH parameterizations can substantially limit their efficiency, as this value might not overcome the threshold diameter that can initiate effective SIP.

Overall, BR is substantially more effective than any other SIP mechanism, but its efficiency highly depends on the treatment of the correction factor ψ, which is included in the Phillips et al. (2017a) parameterization to account for the ice enhancement due to sublimation. This is an unconstrained parameter, while the value assigned by Phillips et al. (2017a) likely results in underestimations of the BR effect. DSH and SUBBR are the two mechanisms with the weakest efficiency in the examined conditions. Moreover, modifications in the HM description to account for rain-snow collisions do not enhance the efficiency of the process. HM and DSH are likely limited by the fact that relatively large raindrops are generally few in the examined conditions. SUBBR is likely not favored due to the high relative humidity conditions that often persist in polar environments. However, it is worth noting that the current SUBBR implementations concern only snow particles that can undergo sublimation break-up only within a limited temperature range (see Section 2c). In contrast, sublimation break-up of graupels can occur at any temperature (Deshmukh et al. 2022). Since this particle category is not treated by MG2, the overall efficiency of the SUBBR mechanism might be underestimated in our simulations.

Interestingly, SIP efficiency increases substantially with decreasing ice aggregation in our simulations. This is because enhanced SIP results in enhanced ice aggregation when a constant aggregation efficiency is assumed. However, in reality, this might not be necessarily true as enhanced SIP may lead to the prevalence of small ice particles that are not efficient in aggregation or to the reduction of dendritic ice crystal concentrations through break-up; dendrites are the ice habits that are known to be most favorable for aggregation (Karrer et al., 2021; Chellini et al., 2021). Nevertheless, our simulations indicate that a good agreement with macrophysical observations from Ny-Ålesund is only achieved in the simulations with enhanced BR and qualitatively constrained aggregation. It is worth noting that with this set-up, the choice of PIP scheme does not play an important role, as SIP efficiency dominates over PIP.

Another interesting finding in our study is that the simulations with significantly enhanced ice production result in increased supercooled liquid water in Ny-Alesund and increased total cloud cover over the whole Arctic region. This is in contrast to the general consensus that increasing ice content is more likely to lead to liquid depletion through the WBF process. Our results show that in some cases a significant shift of the frozen hydrometeor spectra to smaller sizes can result in ice particles that grow less efficiently riming and occasionally less efficient WBF process. Overall, our modification in SIP and ice aggregation results in improved downward radiation compared to observations during the dark and cold months. This is because the enhanced cloud cover in these simulations enhances downward longwave emission, decreasing the negative LWD bias that is produced by the standard NorESM2 model between November-April.

Acknowledgements:

This study is supported by the H2020-EU.1.3.- EXCELLENT SCIENCE - Marie-Skłodowska-Curie Actions project SIMPHAC (ID 8985685), the project IC-IRIM project (ID 2018-01760) funded by the Swedish Research Council for Sustainable Development (FORMAS) and the project FORCeS funded from Horizon H2020-EU.3.5.1. (ID 821205). We are grateful to Øyvind Seland for providing the NorESM2 code, to Inger Helen Karset for providing python scripts to convert ERA-I data to a format readable by NorESM2 and to Dirk Jan Leo Olivie for further clarifications regarding the model. We are also grateful to the scientists that collected and processed Ny-Ålesund observations and especially to Dr. Tatiana Nomokonova for providing clarifications regarding the datasets. The simulations were enabled by resources provided by the Swedish National Infrastructure for Computing (SNIC) at the National Supercomputer Center (NSC), partially funded by the Swedish Research Council through grant agreement no. 2018-05973.

Data availability statement:

Both surface-based and satellite observations are available online. LWP datasets from Ny-Ålesund for the years 2016, 2017 and 2018 can be found at https://doi.org/10.1594/PANGAEA.902096 (Nomokonova et al. 2019a), https://doi.org/10.1594/PANGAEA.902098 (Nomokonova et al. 2019b) and https://doi.org/10.1594/PANGAEA.902099 (Nomokonova et al. 2019c). IWC and Ri_{eff} data can be found at https://doi.pangaea.de/10.1594/PANGAEA.898556 (Nomokonova et al.

2019d). HATPRO temperature profiles can be downloaded from https://doi.org/10.1594/PANGAEA.902145 (Nomokova et al. 2019e), https://doi.org/10.1594/PANGAEA.902146 (Nomokova et al. 2019f) and https://doi.org/10.1594/PANGAEA.902147 (Nomokova et al. 2019g). Ny-Ålesund IWV measurements for the same years are available at https://doi.org/10.1594/PANGAEA.902140 (Nomokonova et al. 2019h), https://doi.org/10.1594/PANGAEA.902142 (Nomokova et al. 2019i) and https://doi.org/10.1594/PANGAEA.902143 (Nomokova et al. 2019j). CVI measurements are available at https://doi.org/10.17043/zeppelin-cloud-aerosol-1 (Karlsson et al. 2021b). The CERES-EBAF data are retrieved from https://ceres.larc.nasa.gov/data/, while GOCCP dataset can be downloaded from https://climserv.ipsl.polytechnique.fr/cfmip-obs/. ERA-Interim reanalysis products can be accessed through https://www.ecmwf.int/en/forecasts/datasets/reanalysis datasets/era-interim.

Appendix A: Sublimation corrector factor in BR formulation

The Phillips et al. (2017a) parameterization predicts the number of fragments (F_{BR}) generated from mechanical break-up upon collisions of two ice particles using the equation:

$$F_{BR} = \alpha A \left(1 - exp\left\{-\left[\frac{CK_o}{\alpha A}\right]^{\gamma}\right\}\right)$$

where K_o is the collisional kinetic energy, α is the surface area of the smaller ice particle that undergoes fracturing, A represents the number density of the breakable asperities in the region of contact, γ is a function of the particle's rimed fraction and C is the asperity-fragility coefficient, which is a function of a correction term (ψ) for the effects of sublimation based on the field observations by Vardiman (1978). Specifically, for planar ice the assigned values are: $C = 7.08 \times 10^6 \psi$ and $\psi = 3.5 \times 10^{-3}$. Thus, a ψ value smaller than unity has a decreasing impact on F_{BR} estimation. Setting ψ=1 in the sensitivity simulations with 'ψ' suffix assumes no impact of sublimation break-up on the Vardiman (1978) data used to constrain the above formulation.

References:

Bacon, N. J., B. D. Swanson, M. B. Baker, and E. J. Davis, 1998: Breakup of levitated frost particles. *J. Geophys. Res.*, **103**, 13 763–13 775, doi: 10.1029/98JD01162.

Bailey, M. P., and J. Hallett, 2009: A comprehensive habit diagram for atmospheric ice crystals: Confirmation from the laboratory, AIRS II, and other field studies. *J. Atmos. Sci.*, **66**, 2888–2899, doi:10.1175/2009JAS2883.1.

Barrett, A. I., C. D. Westbrook, J. C. Nicol, and . H. M Stein, 2019: Rapid ice aggregation process revealed through triple-wavelength Doppler spectrum radar analysis, *Atmos. Chem. Phys.*, **19**, 5753–5769, doi:10.5194/acp-19-5753-2019

Bigg, E. K.: The supercooling of water, *Proc. Phys. Soc. B*, **66**, 688– 694, 1953.

Boucher, O., and Coauthors, 2013: Clouds and aerosols. In *Climate Change 2013: The Physical Science Basis. Contribution of Working Group I to the Fifth Assessment Report of the Intergovernmental Panel on Climate Change* Stocker, T.F. and Coauthors, Eds. Cambridge University Press, pp. 571-657, doi: 10.1017/CBO9781107415324.016.

Chepfer, H., S. Bony, D. Winker, G. Cesana, J. L. Dufresne, P. Minnis, C. J. Stubenrauch, and S. Zeng, 2010: The GCM-Oriented CALIPSO Cloud Product (CALIPSO-GOCCP), *J. Geophys. Res.*, **115**, D00H16, doi: 0.1029/2009JD012251

Connolly, P. J., C. Emersic, and P. R. Field, 2012: A laboratory investigation into the aggregation efficiency of small ice crystals, Atmos. Chem. Phys., 12, 2055–2076, https://doi.org/10.5194/acp-12-2055-2012.

Cotton, W.R. , G.J. Tripoli, R.M. Rauber, and E.A. Mulvihill, 1986: Numerical simulation of the effects of varying ice crystal nucleation rates and aggregation processes on orographic snowfall, *J. Climate Appl. Meteorol.*, **25**, 1658-1680, doi.org/10.1175/1520-0450(1986)025<1658:NSOTEO>2.0.CO;2

Chellini, G., R. Gierens, T. Kiszler, V. Schemann, and S. Kneifel, 2021: Enhanced aggregation observed in Arctic shallow mixed-phase clouds at e between 015 and -10^{o}C, AGU Fall Meeting, December 13-17, New Orleans, Louisiana

Dee D.P., and Coauthors, 2011: The ERA-Interim reanalysis: configuration and performance of the data assimilation system, *Q.J.R. Meteorol. Soc.*, **137**, 553-597, doi.org/10.1002/qj.828

Delanoë, J. ,and R. J. Hogan, 2010: Combined CloudSat-CALIPSO-MODIS retrievals of the properties of ice clouds, *J. Geophys. Res.*, **115**, D00H29, doi: 10.1029/2009JD012346

Deshmukh, A., V. T. J. Phillips, A. Bansemer, S. Patade, and D. Waman, 2022: New Empirical Formulation for the Sublimational Breakup of Graupel and Dendritic Snow, *J. Atmos. Sci.*, **79**, 317–336, doi:10.1175/JAS-D-20-0275.1

Ebell, K., T. Nomokonova, M. Maturilli, and C. Ritter, 2020: Radiative Effect of Clouds at Ny-Ålesund, Svalbard, as Inferred from Ground-Based Remote Sensing Observations, *J. Appl. Meteor. Clim.*, **59**(1), 3-22, doi: 10.1175/JAMC-D-19-0080.1

Field., P., and Coauthors, 2017: Chapter 7: Secondary ice production - current state of the science and recommendations for the future, Meteor. Monogr., **58**, 7.1–7.20 doi: 10.1002/2015GL065497

Gayet, J.-F., R. Treffeisen, A. Helbig, J. Bareiss, A. Matsuki, A. Herber, A. Schwarzenboeck, 2009: On the onset of the ice phase in boundary layer Arctic clouds, *J. Geophys. Res.*, **114**, D19201, doi: 10.1029/2008jd011348

Georgakaki, P., G. Sotiropoulou, É. Vignon, A. C. Billault-Roux, A. Berne, and A. Nenes, 2022: Secondary ice production processes in wintertime alpine mixed-phase clouds, Atmos. Chem. Phys., **22**, 1965–1988, doi: 10.5194/acp-22-1965-2022

Gettelman, A., and H. Morrison, 2015: Advanced Two-Moment Bulk Microphysics for Global Models. Part I: Off-Line Tests and Comparison with Other Schemes, *J. Clim.*, **28**(3), 1268-1287, doi: 10.1175/JCLI-D-14-00102.1

Hallett, J., and S. C. Mossop, 1974: Production of secondary ice particles during the riming process, *Nature*, **249**, 26–28, doi: 10.1038/249026a0

Hogan, R. J., M. P. Mittermaier, and A. J. Illingworth, 2006: The Retrieval of Ice Water Content from Radar Reflectivity Factor and Temperature and Its Use in Evaluating a Mesoscale Model, *J. Appl. Meteor. Clim.*, **45**(2), 301-317, doi: 10.1175/JAM2340.1

Hoose, C., J. E. Kristjánsson, J.-P. Chen, and A. Hazra, 2010: A classical-theory-based parameterization of heterogeneous ice nucleation by mineral dust, soot, and biological particles in a global climate model. *J. Atmos. Sci.*, **67**(8), 2483–2503, doi: 10.1175/2010JAS3425.1

Hoose, C., and O. Möhler, 2012: Heterogeneous ice nucleation on atmospheric aerosols: a review of results from laboratory experiments, *Atmos. Chem. Phys.*, **12**, 9817–9854, doi: 10.5194/acp-12-9817-2012

Illingworth, J., and Coauthors, 2007: Cloudnet, *Bull. Amer. Meteor. Soc.*, **88**(6), 883-898, doi: 10.1175/BAMS-88-6-883

Karlsson, L., R. Krejci, M. Koike, K. Ebell, and P. Zieger, 2021a: A long-term study of cloud residuals from low-level Arctic clouds, Atmos. Chem. Phys., **21**, 8933–8959, doi:10.5194/acp-21-8933-2021

Karlsson, L., R. Krejci, M. Koike, K. Ebell, and P. Zieger, 2021b: Arctic cloud and aerosol measurements from Zeppelin Observatory, Svalbard, November 2015 to February 2018. Dataset version 1. Bolin Centre Database. https://doi.org/10.17043/zeppelin-cloud-aerosol-1

Karrer, M., A. Seifert, D. Ori, and S. Kneifel, 2021: Improving the representation of aggregation in a two-moment microphysical scheme with statistics of multi-frequency Doppler radar observations, Atmos. Chem. Phys., **21**, 17133–17166, doi:10.5194/acp-21-17133-2021

Kato, S., and Coauthors, 2018: Surface Irradiances of Edition 4.0 Clouds and the Earth's Radiant Energy System (CERES) Energy Balanced and Filled (EBAF) Data Product, *Journal of Climate*, **31**(11), 4501-4527, doi: 10.1175/JCLI-D-17-0523.1

Keinert, A., D. Spannagel, T. Leisner, and A. Kiselev, 2020: Secondary Ice Production upon Freezing of Freely Falling Drizzle Droplets, *J. Atmos. Sci.*, **77**(8), 2959-2967, doi: 10.1175/JAS-D-20-0081.1

Kirkevåg, A., and Coauthors, 2018: A production-tagged aerosol module for Earth system models, OsloAero5.3 – extensions and updates for CAM5.3-Oslo, Geosci. Model Dev., **11**, 3945–3982, doi:10.5194/gmd-11-3945-2018.

Korolev, A., and T. Leisner, 2020: Review of experimental studies of secondary ice production, *Atmos. Chem. Phys.*, **20**, 11767–11797, doi: 10.5194/acp-20-11767-2020

Lauber, A., A. Kiselev, T. Pander, P. Handmann, and T. Leisner, 2018a: Secondary ice formation during freezing of levitated droplets, *J. Atmos. Sci.*, **75**, 2815–2826, doi: 10.1175/JAS-D-18-0052.1

Lamb, D. and J. Verlinde, 2011: Physics and Chemistry of Clouds. Cambridge University Press, Cambridge, doi: 10.1017/CBO9780511976377

Lawson, R. P, S. Woods, and H. Morrison., 2015: The microphysics of ice and precipitation development in tropical cumulus clouds. *J. Atmos. Sci.*, **72**, 2429–2445, doi:/10.1175/JAS-D-14-0274.1

Lloyd, G., and Coauthors, 2015: Observations and comparisons of cloud microphysical properties in spring and summertime Arctic stratocumulus clouds during the ACCACIA campaign, *Atmos. Chem. Phys.*, **15**, 3719–3737, doi: 10.5194/acp-15-12953-2015

Luke, E.P., F. Yang, P. Kollias, A.M. Vogelmann, and M.,Maahn, 2021: New insights into ice multiplication using remote-sensing observations of slightly supercooled mixed-phase clouds in the Arctic. *Proceedings of the National Academy of Sciences,* **118**. doi: 10.1073/pnas.2021387118

Meyers, M. P., P. J. DeMott, and W.R. Cotton, 1992: New Primary Ice-Nucleation Parameterizations in an Explicit Cloud Model. *Journal of Applied Meteorology (1988-2005)*, **31**(7), 708–721, http://www.jstor.org/stable/26186583

Mizuno, H., 1990: Parameterization if the accretion process between different precipitation elements. *J. Meteor. Soc. Japan*, **57**, 273-281, doi: 10.2151/jmsj1965.68.3_395

Morrison, H., J.A. Curry, V.I. Khvorostyanov, 2005: A New Double-Moment Microphysics Parameterization for Application in Cloud and Climate Models. Part I: Description, *Atmos. Sci.,* **62***,* 3683-3704, doi: 10.1175/JAS3446.1

Morrison, H., G. De Boer, G. Feingold, J. Harrington, M.D. Shupe, and K. Sulia, 2012: Resilience of persistent Arctic mixed-phase clouds, Nat. Geosci., **5**, 11–17, doi: 10.1038/ngeo1332

Murray, B. J., K. S. Carslaw, and P. R. Field, 2021: Opinion: cloud- phase climate feedback and the importance of ice- nucleating particles, Atmos. Chem. Phys., **21**(2), 665– 679, doi: 10.5194/acp-21-665-2021

Nomokonova, T., C. Ritter, and K. Ebell, 2019a: Liquid water path of HATPRO microwave radiometer at AWIPEV, Ny-Ålesund (2016). PANGAEA, doi: 10.1594/PANGAEA.902096

Nomokonova, T., C. Ritter, and K. Ebell, 2019b: Liquid water path of HATPRO microwave radiometer at AWIPEV, Ny-Ålesund (2017). PANGAEA, doi: 10.1594/PANGAEA.902098

Nomokonova, T., C. Ritter, and K. Ebell, 2019c: Liquid water path of HATPRO microwave radiometer at AWIPEV, Ny-Ålesund (2017). PANGAEA, doi: 10.1594/PANGAEA.902099

Nomokonova, T., and K. Ebell, 2019d: Cloud microphysical properties retrieved from ground-based remote sensing at Ny-Ålesund (10 June 2016 - 8 October 2018). University of Cologne, PANGAEA, doi: 10.1594/PANGAEA.898556

Nomokonova, T., C. Ritter, and K. Ebell, 2019e: Temperature profile of HATPRO microwave radiometer at AWIPEV, Ny-Ålesund (2016). PANGAEA, doi: 10.1594/PANGAEA.902145

Nomokonova, T., C. Ritter, and K. Ebell, 2019f: Temperature profile of HATPRO microwave radiometer at AWIPEV, Ny-Ålesund (2017). PANGAEA, doi: 10.1594/PANGAEA.902146

Nomokonova, T., C. Ritter, and K. Ebell, 2019g: Temperature profile of HATPRO microwave radiometer at AWIPEV, Ny-Ålesund (2018). PANGAEA, doi: 10.1594/PANGAEA.902147

Nomokonova, T., C. Ritter, and K. Ebell, 2019h: Integated water vapor of HATPRO microwave radiometer at AWIPEV, Ny-Ålesund (2016). PANGAEA, doi: 10.1594/PANGAEA.902140

Nomokonova, T., C. Ritter, and K. Ebell, 2019i: Integated water vapor of HATPRO microwave radiometer at AWIPEV, Ny-Ålesund (2017). PANGAEA, doi: 10.1594/PANGAEA.902142

Nomokonova, T., C. Ritter, and K. Ebell, 2019j: Integated water vapor of HATPRO microwave radiometer at AWIPEV, Ny-Ålesund (2018). PANGAEA, doi: 10.1594/PANGAEA.902143

Oraltay, R., and J. Hallett, 1989: Evaporation and melting of ice crystals: A laboratory study. *Atmos. Res.*, **24**, 169–189, doi:10.1016/0169-8095(89)90044-6

Pasquier, J. T., and Coauthors, 2022: Conditions favorable for secondary ice production in Arctic mixed-phase clouds, Atmos. Chem. Phys. Discuss. [preprint], https://doi.org/10.5194/acp-2022-314

Passarelli, R. E., 1978: An Approximate Analytical Model of the Vapor Deposition and Aggregation Growth of Snowflakes, *J. Atmos. Sci.*, **35**(1), 118-124, doi: 0.1175/1520-0469(1978)035<0118:AAAMOT>2.0.CO;2

Phillips, V. T. J., M. Formenton, A. Bansemer, I. Kudzotsa, and B. Lienert, 2015). A Parameterization of Sticking Efficiency for Collisions of Snow and Graupel with Ice Crystals: Theory and Comparison with Observations, *J. Atmos. Sci.*, **72**(12), 4885-4902.

Phillips, V. T. J, J. I. Yano, A. Khain, 2017a: Ice multiplication by breakup in ice-ice collisions. Part I: Theoretical formulation, *J. Atmos. Sci.*, **74**, 1705 1719, doi: 10.1175/JAS-D-16-0224.1

Phillips, V. T. J., J. I. Yano, M. Formenton, E. Ilotoviz, V. Kanawade, I. Kudzotsa, J. Sun, A. Bansemer, A.G. Detwiler, A. Khain, and S.A., Tessendorf, 2017b: Ice multiplication by breakup in ice-ice collisions. Part II: Numerical simulations, J. Atmos. Sci., **74**, 2789–2811,doi: 10.1175/JAS-D-16-0223.1

Phillips, V. T. J., S. Patade, J. Gutierrez, and A. Bansemer, 2018: Secondary Ice Production by Fragmentation of Freezing Drops: Formulation and Theory, *J. Atmos. Sci.*, **75**(9), 3031-3070, doi:10.1175/JAS-D-17-0190.1

Rangno, A.L., and P.V. Hobbs, 2001: Ice particles in stratiform clouds in the Arctic and possible mechanisms for the production of high ice concentrations, *J. Geophys. Res.*, **106**, 15065–15075, doi: 10.5194/acp-19-5293-2019

Reisner, J., R. M. Rasmussen, and R. T. Bruintjes, 1998: Explicit forecasting of supercooled liquid water in winter storms using the MM5 mesoscale model, *Quart. J. Roy. Meteor. Soc.*, **124**(548), 1071-1107, doi: 10.1002/qj.49712454804

Schwarzenboeck, A., V. Shcherbakov, R. Lefevre, J. F. Gayet, Y. Pointin, and C. Duroure, 2009: Indications for stellar-crystal fragmentation in Arctic clouds, Atmos. Res., **92,** 220–228, doi: 10.1016/j.atmosres.2008.10.002

Seinfeld J. H., and Coauthors, 2016: Improving our fundamental understanding of the role of aerosol-cloud interactions in the climate system. *Proc. Natl. Acad. Sci. USA*, **113**(21), 5781–5790, doi:10.1073/pnas.1514043113

Seland, Ø., and Coauthors, 2020: Overview of the Norwegian Earth System Model (NorESM2) and key climate response of CMIP6 DECK, historical, and scenario simulations, *Geosci. Model Dev.*, **13**, 6165–6200, doi: 10.5194/gmd-13-6165-2020

Shaw, J., Z. McGraw, O. Bruno, T. Storelvmo, and S. Hofer, 2022: Using satellite observations to evaluate model microphysical representation of Arctic mixed-phase clouds. *Geophysical Research Letters*, **49**, e2021GL096191. doi: 10.1029/2021GL096191

Shupe, M. D, S. Y. Matrosov, and T. Uttal, 2006: Arctic Mixed-Phase Cloud Properties Derived from Surface-Based Sensors at SHEBA, *J. Atmos. Sci.*, **63**(2), 697-711, doi: 10.1175/JAS3659.1

Shupe, M. D., V. P. Walden, E. Eloranta, T. Uttal, J. R. Campbell, S. M. Starkweather, and M. Shiobara, 2011: Clouds at Arctic at- mospheric observatories. Part I: Occurrence and macro- physical properties. J. Appl. Meteor. Climatol., **50**, 626–644, doi:10.1175/2010JAMC2467.1.

Sledd, A., and T. L'Ecuyer, 2021: Uncertainty in Forced and Natural Arctic Solar Absorption Variations in CMIP6 Models, *Journal of Climate*, **34(**3), 931-948. 10.1175/JCLI-D-20-0244.1

Storelvmo, T., 2017: Aerosol Effects on Climate via Mixed-Phase and Ice Clouds. *Annual Review of Earth and Planetary Sciences,* **45**, 199-222, doi:10.1146/ANNUREV-EARTH-060115-012240

Sotiropoulou, G., S. Sullivan, J. Savre, G. Lloyd, T. Lachlan-Cope, A. M. L. Ekman, and A. Nenes, 2020: The impact of secondary ice production on Arctic stratocumulus, Atmos. Chem. Phys., **20**, 1301–1316, doi: 10.5194/acp-20-1301-2020

Sotiropoulou, G., É. Vignon, G. Young, H. Morrison, S. J. O'Shea, T. Lachlan-Cope, A. Berne, and A. Nenes, 2021a: Secondary ice production in summer clouds over the Antarctic coast: an underappreciated process in atmospheric models, Atmos. Chem. Phys., **21**, 755–771, doi: 10.5194/acp-21-755-2021

Sotiropoulou, G., L. Ickes, A. Nenes, A., and A.M.L. Ekman, 2021b: Ice multiplication from ice–ice collisions in the high Arctic: sensitivity to ice habit, rimed fraction, ice type and uncertainties in the numerical description of the process, Atmos. Chem. Phys., **21**, 9741–9760, doi: 10.5194/acp-21-9741-2021.

Sullivan, S. C., A. Kiselev, T. Leisner, C. Hoose, ans A. Nenes, 2018: Initiation of secondary ice production in clouds, *Atmos. Chem. Phys.*, **18**, 1593–1610, doi: 10.5194/acp-18-1593-2018

Takahashi, T., Y. Nagao, and Y. Kushiyama, 1995: Possible high ice particle production during graupel-graupel collisions, J. Atmos. Sci., **52**, 4523–4527

Tan, I., and T. Storelvmo, 2019: Evidence of strong contributions from mixed-phase clouds to Arctic climate change. *Geophys. Res. Let.*, **46**, 2894– 2902, doi: 10.1029/2018GL081871

Thomas, M. A., A. Devasthale, T. L'Ecuyer, S. Wang, T. Koenigk and K. Wyser, 2019: Snowfall distribution and its response to the Arctic Oscillation: an evaluation of HighResMIP models in the Arctic using CPR/CloudSat observations, Geosci. Model Dev., **12**, 3759–3772, doi:10.5194/gmd-12-3759-2019

Vardiman, L., 1978: The generation of secondary ice particles in clouds by crystal-crystal collision, J. *Atmos. Sci.*, **35**, 2168–2180, doi: 0.1175/1520-0469(1978)035<2168:TGOSIP>2.0.CO;2,

Vignesh, P. P., J. H. Jiang, P. Kishore, H. Su, T. Smay, N. Brighton, and I. Velicogna, 2020: Assessment ofCMIP6 cloud fraction and comparisonwith satellite observations.Earth and Space Science, **7**, e2019EA000975. doi: 10.1029/2019EA000975

Wang, Y., X. Liu, C. Hoose, C., and B. Wang, 2014: Different contact angle distributions for heterogeneous ice nucleation in the Community Atmospheric Model version 5. *Atmos. Chem. Phys.*, **14**(19), 10411–10430, doi: 10.5194/acp-14-10411-2014

Wex, H., and Coauthors, 2019: Annual variability of ice-nucleating particle concentrations at different Arctic locations, *Atmos. Chem. Phys.*, **19**, 5293-5311, doi:10.5194/acp-19-5293-2019

Wielicki, B. A., B. R. Barkstrom, E. F. Harrison, R. B. III Lee, G. L. Smith, and J. E. Cooper, 1996: Clouds and the Earth's Radiant Energy System (CERES): An Earth Observing System Experiment, *Bull. Amer. Meteorol. Soc.*, **77**(5), 853-868, doi: ulletin of the American Meteorological Society, **77**(5), 853-868, doi: 10.1175/1520-0477(1996)077<0853:CATERE>2.0.CO;2.

Young, K. C., 1974: The Role of Contact Nucleation in Ice Phase Initiation in Clouds, *Journal of Atmospheric Sciences*, **31**(3), 768-776.

Zelinka, M. D., and Coauthors, 2020: Causes of higher climate sensitivity in CMIP6 models. Geophys. Res. Lett., **47**, e2019GL085782, doi:10.1029/2019GL085782.

Zhao, X., X. Liu, V. T. J. Phillips, and S. Patade, 2021: Impacts of secondary ice production on Arctic mixed-phase clouds based on ARM observations and CAM6 single-column model simulations, *Atmos. Chem. Phys.*, **21**, 5685–5703, doi: 10.1029/2021GL092581

Zhao, X., and X. Liu, 2021: Global importance of secondary ice production. *Geophys. Res. Let.*, **48**, e2021GL092581, doi: 10.1029/2021GL092581

Zhao, X., and X. Liu, 2022: Relative importance and interactions of primary and secondary ice production in the Arctic mixed-phase clouds*, Atmos. Chem. Phys.*, **22**, 2585–2600, doi: 10.5194/acp-2021-686